Maskless Micro/Nanopatterning and Bipolar Electrical-Rectification of MoS2 Flakes Through Femtosecond Laser Direct Writing

Journal:	*ACS Applied Materials & Interfaces*
Manuscript ID	Draft
Manuscript Type:	Article
Date Submitted by the Author:	n/a
Complete List of Authors:	Zuo, Pei; Beijing Institute of Technology, Jiang, Lan; Beijing Institute of Technology, School of Mechanical Engineering Li, Xin; Beijing Institute of Technology, Department of Mechanical & Automation Engineering Tian, Mengyao; Beijing Institute of Technology Xu, Chenyang; Beijing Institute of Technology Yuan, Yongjiu; Beijing Institute of Technology Ran, Peng; Beijing Institute of Technology Li, Bo; Beijing Institute of Technology, Lu, Yong Feng; University of Nebraska-Lincoln, Electrical Engineering

Maskless Micro/Nanopatterning and Bipolar Electrical-Rectification of MoS_2 Flakes Through Femtosecond Laser Direct Writing

Pei Zuo,[†] Lan Jiang, [†] Xin Li, [,†] Mengyao Tian, [†] Chenyang Xu, [†] Yongjiu Yuan, [†] Peng Ran, [†] Bo Li, [†] Yongfeng Lu,[§]*

[†]Laser Micro/Nano Fabrication Laboratory, School of Mechanical Engineering, Beijing Institute of Technology, Beijing 100081, P.R. China, [§]Laser Assisted Nano Engineering Laboratory, Department of Electrical and Computer Engineering, University of Nebraska-Lincoln, Lincoln, NE 68588-0511, USA

KEYWORDS: MoS_2 flakes, femtosecond laser direct writing, micro/nanopatterning, oxygen bonding, electrical rectification

ABSTRACT: MoS_2 micro/nanostructures are desirable for tuning electronic properties, developing required functionality, and improving existing performance of multilayer MoS_2 devices. This work presents a useful method to flexibly microprocess multilayer MoS_2 flakes through femtosecond laser pulse direct writing, which can directly fabricate regular MoS_2 nanoribbon arrays with ribbon widths of 179, 152, 116, 98, and 77 nm, and arbitrarily pattern MoS_2 flakes to form micro/nanostructures such as single nanoribbon, labyrinth array, and cross structure. This method is mask-free and simple, and has high flexibility, strong controllability, and high precision.

Moreover, numerous oxygen molecules are chemically and physically bonded to laser-processed MoS_2, attributed to roughness defect-sites and edges of micro/nanostructures that contain numerous unsaturated edge-sites and highly active centres. In addition, electrical tests of the field effect transistor fabricated from prepared MoS_2 nanoribbon arrays reveal new interesting features: output and transfer characteristics exhibit strong rectification (not going through zero and bipolar conduction) of drain−source current, which is supposedly attributed to the coordinate structures and p-type chemical doping of oxygen molecules on MoS_2 nanoribbon arrays. This work demonstrates the ability of femtosecond laser pulses to directly induce micro/nanostructures, property changes, and new device-properties of two-dimension materials, which may future enable new device applications.

INTRODUCTION

Transition metal dichalcogenides (TMDCs), representative layered materials like graphene, have been widely studied as a family of new-type semiconducting materials with extraordinary mechanical, electrical, and optical properties, and great promise for extensive applications.[1-6] Molybdenum disulfide (MoS_2), representative material belonging to the TMDC group, has lattice structure of a layer of molybdenum atoms sandwiched between two layers of sulfur atoms.[7-8] Unlike graphene with zero-band-gap, MoS_2 is a band-gap semiconductor with sizable energy band gap:[5, 9] MoS_2 in bulk form has indirect energy gap of ~1.2 eV and MoS_2 in monolayer form has direct band gap of ~1.8 eV.[3] Hence, MoS_2 can serve as a promising candidate of graphene, and has excellent potential in semiconductor-related applications of layered

materials such as thin-film transistors,[1, 10] integrated circuits,[11-12] complementary inverter,[13] photodetectors,[14] light-emitting diodes,[15-16] photovoltaics,[17-18] superconductors,[19-20] and chemical/biological sensors.[21-22]

To achieve desirable electronic properties and required functionality and improve existing performance of MoS_2 devices, a microfabrication process is usually required to fabricate large arrays of orderly arranged MoS_2 micro/nanostructures, commonly involving patterning and etching.[3, 23] Hence, it is crucial to conduct research on MoS_2 patterning with ordered micro/nanostructures, controlled structure-size, and device application having new features. Several approaches have been attempted to pattern MoS_2 materials or fabricate micro/nanostructures of MoS_2 deposited on substrates, including tape exfoliation,[24-25] chemical vapor deposition (CVD),[26-27] thermal decomposition of thiosalts,[28] van der Waals epitaxial growth,[29-30] patterned MoO3 sulfurization,[31-32] CVD in plasma-treated areas,[33-34] block copolymer lithography,[35] reactive ion etching (RIE) combined with deposition in plasma-treated areas,[3] lithography combined with stamping,[23] lithography combined with RIE,[36-37] and continue wave (CW) laser direct processing.[38-39] Among them, CVD in plasma-treated areas, block copolymer lithography, lithography combined with deposition in plasma-treated areas, lithography combined with stamping, lithography combined with RIE, and CW laser direct processing can realize control for the location, shape, and size of MoS_2 micro/nanostructures. Whereas, in the methods involving lithography, plasma surface treatment, and RIE, chemical organics (such as photoresist) and inorganic or organic masks are used, combined process are required,

and the integral process is relatively complex. CW laser direct processing is a one-step process and is simple, no special atmosphere system and mask are needed, cost is relatively low, and flexibility and controllability are high. Whereas, CW laser processing is a thermal process, and the strong thermal effect would cause thermal oxidization of materials and lead to large recasting layer, hence processing precision is insufficient. Femtosecond (ultrafast) laser pulse direct processing is another kind of laser processing technology. Femtosecond laser pulses have ultrashort pulse width, ultrahigh power density, and nonlinear nonequilibrium processing feature, and multiphoton absorption and nonthermal effect can be realized, hence except including almost all the advantages of CW laser processing, femtosecond laser direct processing also possesses high processing precision.[40-41]

In this work, we proposed a useful method of utilizing femtosecond laser pulse direct writing to modify multilayer MoS_2 flakes, directly fabricate regular MoS_2 nanoribbon arrays with different ribbon widths, and arbitrarily pattern MoS_2 flakes to form different MoS_2 micro/nanostructures. Moreover, the laser-fabricated MoS_2 structures were chemically and physically bonded with numerous oxygen molecules in the air, which can be attributed to the roughness defect-sites and long edges of the nanoribbons that may contain numerous unsaturated edge sites and highly active centres. At last, electronic properties of MoS_2 nanoribbon arrays fabricated to be field effect transistor (FET) were tested, and the output and transfer characteristics exhibited strong rectification (not went through zero and exhibited bipolar conduction) of drain−source current. This rectification was supposedly attributed to the coordinate

structures and p-type chemical doping of oxygen molecules on MoS_2 nanoribbon arrays, which may cause transition of n-type channel to p-type channel or properties similar to pn junction. The proposed method had advantages of simplicity, maskless, strong controllability, high flexibility, and high precision, and also indicated the ability of femtosecond laser pulses to directly induce two-dimension micro/nanostructures/patterns, property changes of two-dimension material, and new device features.

RESULTS AND DISCUSSION

In this work, multilayer MoS_2 flakes were mechanically exfoliated from a natural crystal and deposited on 300nm-SiO_2/Si substrates. The thickness of MoS_2 flakes selected for experiments was several to dozens of nanometers. The schematic of our method of fabricating MoS_2 nanoribbons/patterns is shown in Figure 1a, which relies on the formation of regular nanostructures and the material removal by femtosecond laser pulse irradiation. When femtosecond laser pulse beam is focused and irradiated on material surface, surface plasmons (SPs) can be induced on the material surface, interference of which with incident laser field can lead to the formation of initial grating structures on material, then these initial grating structures can assist the coupling of SPs and incident laser field, leading to the further formation of final grating structures with deeper gaps.[42] The depth of gaps of laser induced grating structures is influenced by the number and energy of ultrafast laser pulses on unit area of material, and can be on a micrometer scale.[40, 43-44] The MoS_2 used in our experiment was nano-scale thin flake, therefore controlling scan speed of laser beam

enough slow (laser pulse number on unit area of MoS_2 enough large) can control the gaps penetrating the whole MoS_2 thin flake, enabling surface nanogratings to become independent nanoribbons. Figure 1b shows the optical comparison of pristine MoS_2 with femtosecond laser-processed (FLP-) MoS_2, which showed obviously optical color change of MoS_2 flake after femtosecond laser irradiation, indicating the change in thickness or surface roughness. Figure 1c shows the atomic force microscope (AFM) results of MoS_2 flake in Figure 1b, which indicates a reduction of outline height of FLP-MoS_2 flake, suggesting the thinning effect on MoS_2 by femtosecond laser irradiation. Figure 1d shows the high resolution AFM image of FLP-MoS_2, which indicated the formation of MoS_2 grating structures.

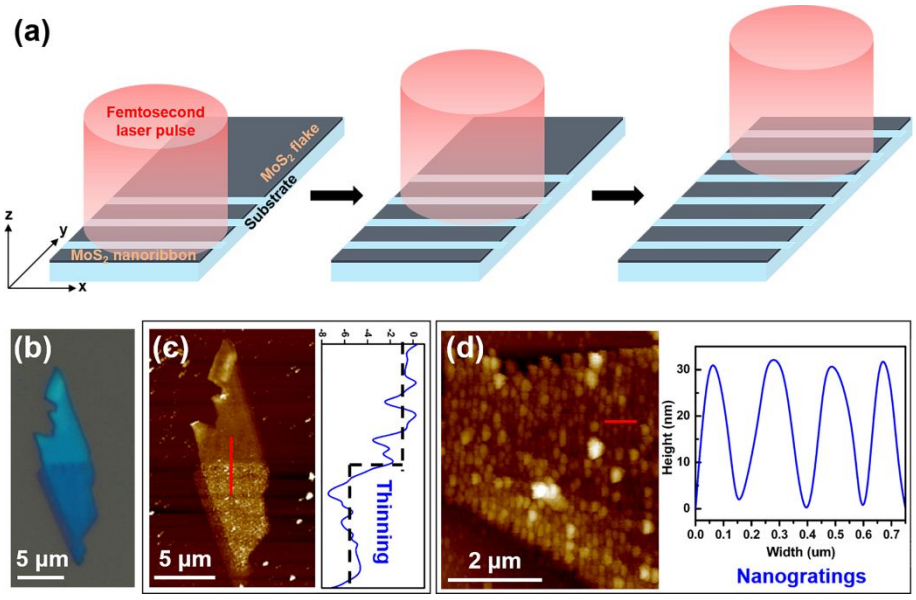

Figure 1. Principle and preliminary characterization of this method. a) Schematic of femtosecond laser direct wiring processing to induce MoS_2 nanoribbons array. b) Optical comparison of pristine MoS_2 (upper part) with FLP-MoS_2 (lower part). c) AFM and d) high resolution AFM of the FLP-MoS_2 flake.

To further investigate the FLP-MoS_2 micro/nanostructures, scanning electron

microscope (SEM) was carried out to characterize its physical morphology, as shown in Figure 2. Figure 2a-e show regular MoS_2 nanoribbon arrays with different ribbon widths of approximate 179, 152, 116, 98, and 77 nm, respectively. Figure 2f shows two independent MoS_2 nanoribbons with small and big width of 56 and 420 nm, respectively. Figure 2g and h show two kind of MoS_2 patterned structures obtained through material removal by femtosecond laser direct writing, which were a labyrinth array and a cross structure, indicating the flexible processing capability of femtosecond laser for arbitrary patterns.

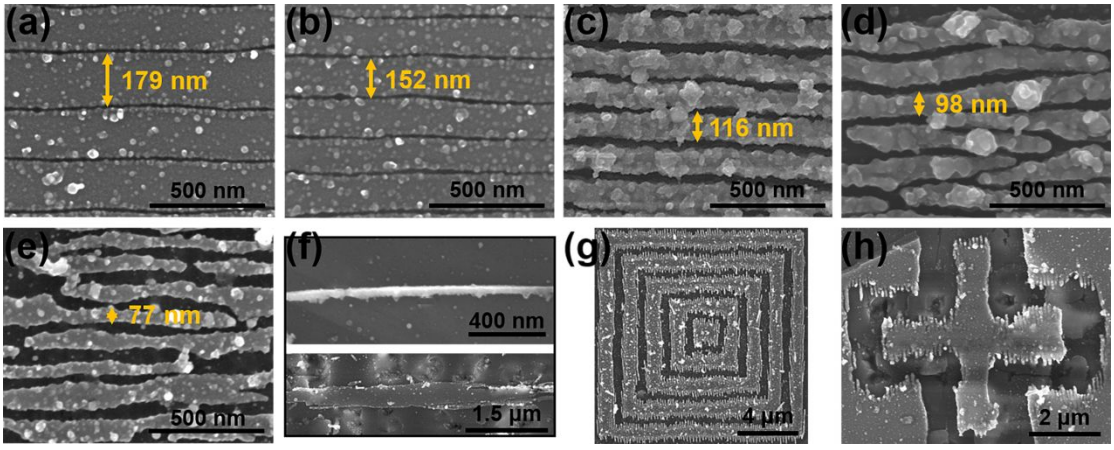

Figure 2. FLP-MoS_2 micro/nanostructures and patterns. a-e) SEM images of regular MoS_2 nanoribbon arrays with widths of 179, 152, 116, 98, and 77 nm, respectively. f) SEM images of two independent MoS_2 nanoribbons with width of (up) 56 and (down) 420 nm. SEM images of g) MoS_2 labyrinth array and h) MoS_2 cross structure.

To investigate the formation of MoS_2 nanoribbons rather than surface structures on MoS_2, energy dispersive X-ray (EDX) analysis was performed. Figure 3a-c show the SEM images of the edge of a FLP-MoS_2 flake, and its S and Si EDX mapping images. The grey part denotes MoS_2, the black part denotes substrate, and the regular stripe structures were obtained through the irradiation of femtosecond laser pulses

(Figure 3a). Figure 3b shows the clearly separated MoS_2 nanoribbons, and Figure 3c shows the clear gaps between these MoS_2 nanoribbons. Figure 3d-f shows the SEM image of MoS_2 nanoribbon arrays, and their S and Si EDX mapping images, which also indicated the separation of MoS_2 nanoribbons, thus evidencing the formation of MoS_2 nanoribbons.

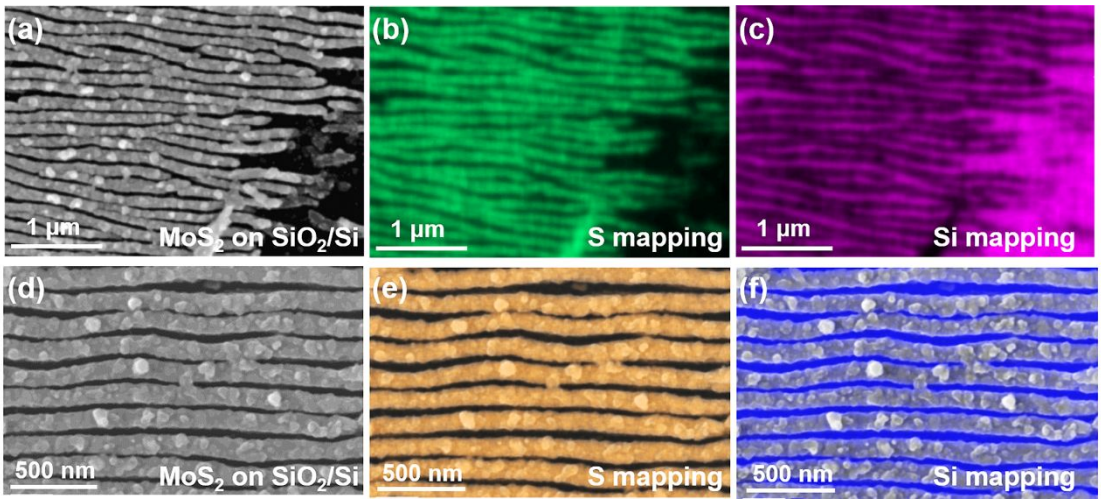

Figure 3. The formation of separated MoS_2 nanoribbons. a) SEM image of the edge of a FLP-MoS_2 flake, and their b) S and c) Si EDX mapping images. d) SEM image of MoS_2 nanoribbon arrays, and their e) S and f) Si EDX mapping images.

To investigate the change in chemical property of FLP-MoS_2 flaks, Raman and X-ray photoelectron spectroscopy (XPS) characterizations were conducted. Figure 4a and d show the Raman spectra of pristine MoS_2 and FLP-MoS_2. There was no Raman peak at 820 cm^{-1} originating from MoO_3, which indicted no formation of MoO_3 thus no obviously thermal oxidation for FLP-MoS_2,[45] due to the non-thermal effect of femtosecond laser processing.[40] No Raman peak of SiO_2 at 520 cm^{-1} was detected on pristine MoS_2 flake, however, there was an obviously Raman peak of SiO_2 was detected on FLP-MoS_2 flake, which indicated that substrate was also detected on

FLP-MoS_2 flake.[46-47] This result also proved the separation of MoS_2 nanoribbons and penetrating gaps between them, which was consistent with the results in Figure 3. XPS Mo and O spectra of pristine MoS_2 and FLP-MoS_2 are also shown in Figure 4 (XPS S spectra for them are shown in Figure S1 and S2). The Mo 3d spectra for pristine MoS_2 is shown in Figure 4b, which reveals three peaks at 227.2, 229.3, and 232.4 eV, respectively assigned to the S 2s orbital of divalent sulfur, and the Mo^{4+} $3d_{5/2}$ and $3d_{3/2}$ orbitals of tetravalent molybdenum. However, in Mo 3d spectra for FLP-MoS_2 (Figure 4e), except the three peaks as shown in pristine MoS_2, there is a new peak at ~235 eV, which is assigned to the Mo^{6+} $3d_{3/2}$ orbital of hexavalent molybdenum. The Mo^{6+} in FLP-MoS_2 was attributed to the Mo−O bonds formed through oxygen bonding to the unsaturated Mo bonds, defect sites, or edge of nanoribbons that generated from the damage and material removal of MoS_2 induced by femtosecond laser pulses,[48-49] Figure 4c shows the O 1s spectra for pristine MoS_2, which reveals two peak at 532.6 and 533.4 eV, attributed to the divalent oxygen of Si–O bonds and the nonvalent oxygen of oxygen molecules physically adsorbed on MoS_2 surface (O_2/MoS_2), respectively.[50-52] The divalent oxygen of Si–O bonds was derived from the 300-nm SiO_2/Si substrate, and oxygen molecules on MoS_2 surface should be attributed to the intrinsic defect and edge of the flake, which were active sites with physical adsorption capacity. However, in O 1s spectra for FLP-MoS_2 (Figure 4f), except the strong and dominant peak assigned to divalent oxygen of Si–O bonds as shown in pristine MoS_2, it revealed stronger peak of nonvalent oxygen of O_2/MoS_2, indicating more oxygen molecules physically adsorbed on MoS_2 surface; it

also revealed a new peak at approximately 530.5 eV assigned to the divalent oxygen of Mo–O bonds,[53-54] which was consistent with the result of XPS Mo 3d spectra. These results indicated that more oxygen atoms/molecules were chemical and physical bonded to FLP-MoS_2. This can be attributed to the roughness defect-sites on MoS_2 nanoribbons and the long edges of these nanoribbons, for they contained numerous unsaturated edge sites and were numerous highly active centres, which can physically and chemically bonded with adsorbates such as O_2 molecules.[55-57] The oxygen absorption on MoS_2 not only led to the change in chemical valence of MoS_2, but also, according to previous reports, can lead p-type doping effect on MoS_2 with O_2 as electron acceptor and MoS_2 as electron donor.[55]

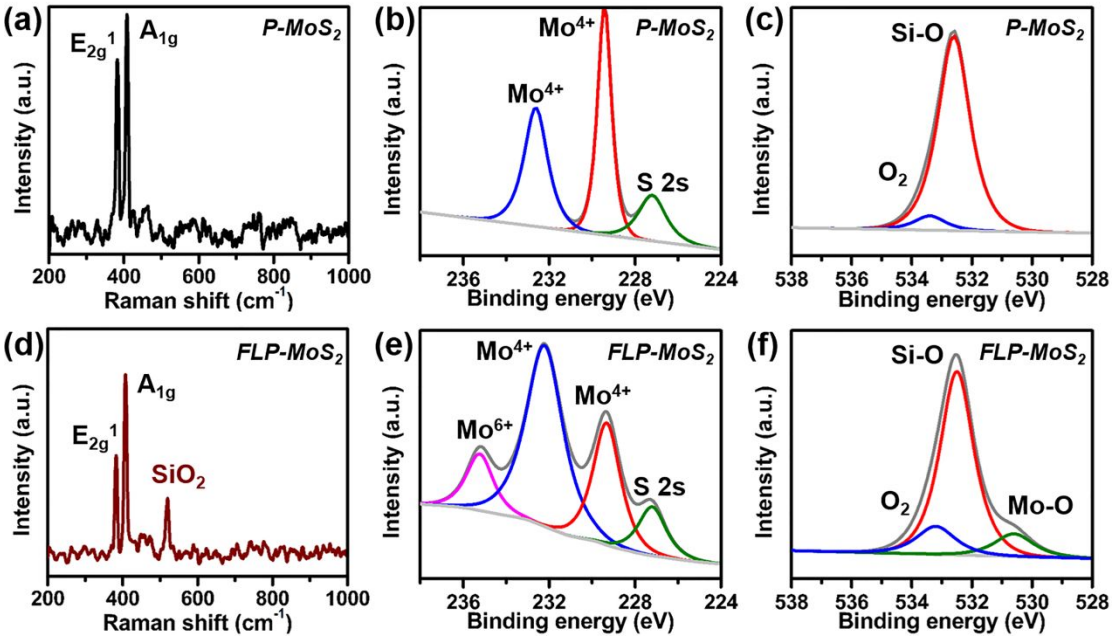

Figure 4. Raman and XPS spectra of P-MoS_2 and FLP-MoS_2. a) Raman spectra of P-MoS_2. XPS peak-split results of b) Mo 3d and c) O 1s spectra of P-MoS_2. d) Raman spectra of FLP-MoS_2. XPS peak-split results of e) Mo 3d and f) O 1s spectra of FLP-MoS_2.

To evaluate the electronic properties of prepared MoS_2 nanoribbon arrays, we

fabricated a back gate FET by using MoS_2 nanoribbon arrays (NrA) on SiO2/p+ Si substrates as channel, with 5 nm Ti/ 75 nm Au as source and drain electrodes, through electron beam lithography (EBL), metal evaporation deposition, and a lift-off process. The electrical measurements of fabricated FET were performed by using a Keithley 4200 semiconductor characterization system in air and at room temperature. The schematic of the structure and measurement of the fabricated MoS_2 NrA-FET is shown in Figure 5a. Figure 5b shows the SEM image of MoS_2 nanoribbon arrays used for fabricating the FET with channel length of $L \approx 3.4$ μm, integral channel width of $W \approx 6.6$ μm, ribbon number of about 38, and gate dielectric thickness of $d = 300$ nm. For comparison, pristine MoS_2 flake was also fabricated as a back-gated FET. Figure 5c shows the drain−source current (I_{DS}) versus drain−source voltage (V_{DS}) characteristics of this NrA-FET under different gate voltages (V_G) ranging from -15 to 15 V. For this output characteristic curve, the drain−source current changed linearly with the drain−source voltage, indicating nearly ohmic contact for this FET device. In addition, the output curve did not go through zero and exhibited a strong rectification of the drain−source current, which was different from the output characteristic curve of the FET fabricated by using pristine/undamaged MoS_2 flake as shown in Figure S3a. This may be attributed to the p-type chemical doping of oxygen molecules on MoS_2 nanoribbon arrays, which might cause transition of n-type channel to p-type channel or properties similar to pn junction.[3]

Figure 5d shows the drain−source current (I_{DS}) versus gate voltages (V_G) characteristics of this NrA-FET under different drain−source voltage (V_{DS}) ranging

from 6 to 10 V. The trend of this transfer curve was non-monotone variation and exhibited a strong rectification of the drain−source current, which was different from the transfer characteristic curve of the FET fabricated by using pristine/undamaged MoS_2 flake. As shown in Figure S3b, the transfer characteristic curve of pristine/undamaged MoS_2 FET exhibited n-type conduction. However, the transfer characteristic curve of MoS_2 NrA-FET exhibits bipolar conduction, similar to p-n type transfer conduction (Figure 5d), with current chopping by a small voltage range. To further evaluate the electronic properties of this device, the on/off ratio, carrier mobility (μ), and subthreshold swing (SS) were calculated. The on/off ratio of the device was calculated to be 1.2×10^2 (p-type segment) and 1.7×10^3 (n-type segment) at the drain−source voltage (V_{DS}) of 10 V. The carrier mobility (μ) was calculated according to the equation from previous reports,[23] as shown in Equation 1,

$$\mu = \frac{L}{W}\frac{d}{\varepsilon_0\varepsilon_r}\frac{1}{V_{DS}}\frac{\partial I_{DS}}{\partial V_G} \quad (1)$$

where L and W are the length and width of FET channel, respectively; d, ε_0, and ε_r are the thickness, vacuum permittivity, and relative permittivity of grid dielectric layer, respectively; $\frac{\partial I_{DS}}{\partial V_G}$ can be calculated from the I_{DS}–V_G curve. For this FET device, the length and width of channel were $L \approx 3.4$ μm and $W \approx 6.6$ μm; the grid dielectric layer was SiO_2, its thickness was $d \approx 300$ nm, and its vacuum permittivity and relative permittivity were $\varepsilon_0 \approx 8.85 \times 10^{-12}$ F/m and $\varepsilon_r \approx 3.9$ F/m,[23] respectively. Hence, the carrier mobility of this device was calculated to be approximately 2.6×10^{-3} $cm^2\ V^{-1}\ s^{-1}$. The SS was calculated according to the equation from previous reports,[58] as

shown in Equation 2,

$$SS = \frac{\Delta V_G}{\Delta \log I_{DS}} \tag{2}$$

and the SS of this device was calculated to be ~21 V/dec according Equation 2. The obvious strong rectification behavior of I_{DS}–V_{DS} and I_{DS}–V_G of the MoS_2 NrA-FET indicated the property change of material and the new device properties, which may enable new device applications. In addition, moderate surface modification of MoS_2 flakes by femtosecond laser pulses would also tune the n-type electronic properties of MoS_2 FET: as shown in Figure S3, the on/off ratio of MoS_2 FET was increased by two magnitude; as shown in Figure S4, the drain−source current (I_{DS}) increased quicker and reached saturation faster with the increase of gate voltages (V_G).

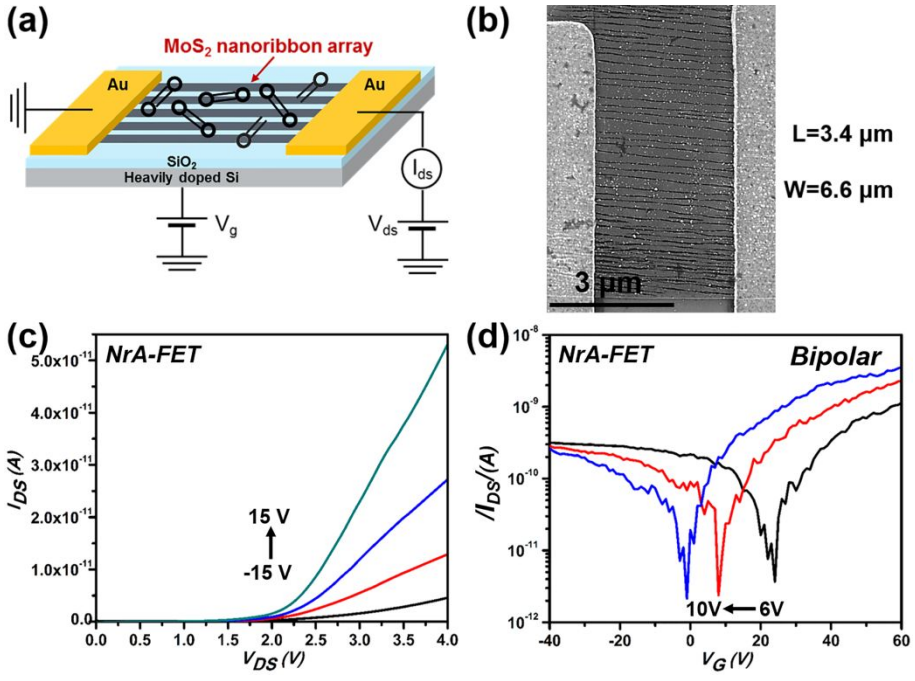

Figure 5. Electrical test of MoS_2 NrA-FET. a) Schematic of the structure and measurement of fabricated MoS_2 NrA-FET. b) SEM image of MoS_2 nanoribbon arrays used for fabricating FET. c) Output and d) transfer characteristic curve of the fabricated MoS_2 NrA-FET.

CONCLUSIONS

Femtosecond laser pulse direct writing was used to nonthermally modify multilayer MoS_2 flakes, induce separated MoS_2 nanoribbon arrays, and arbitrarily pattern MoS_2 flakes to form different MoS_2 micro/nanostructures. Optical microscope, AFM, and SEM were performed to characterize the physical micromorphology of laser processed-MoS_2 flakes. EDX mapping indicated the separation of MoS_2 nanoribbons, proving the formation of MoS_2 nanoribbons rather than surface structures on MoS_2. Raman spectra indicated the non-thermal effect of femtosecond laser processing, also proved the separation of MoS_2 nanoribbons and the penetrating gaps between them. XPS spectra indicated that more oxygen molecules were chemical and physical bonded to FLP-MoS_2, which attributed to the roughness defect sites on MoS_2 nanoribbons and the long edges of the nanoribbons that contained numerous unsaturated edge sites and highly active centres. A MoS_2 NrA-FET was fabricated and electrical tests were conducted to evaluate the electronic properties of prepared MoS_2 nanoribbon arrays. Results indicated that the output and transfer characteristic curves exhibited strong rectification (not going through zero and bipolar conduction) of drain−source current, which were different from that of FET fabricated by using pristine/undamaged MoS_2 flake. This may be attributed the coordinate structures and p-type chemical doping of oxygen molecules on MoS_2 nanoribbon arrays, which might cause transition of n-type channel to p-type channel or properties similar to pn junction. At last, the on/off ratio, carrier mobility, and SS were also calculated. The proposed method indicated the ability of femtosecond laser

pulses to directly induce two-dimension nanostructures, property change in material, and new device properties, which may future enable new device applications.

METHODS

Femtosecond laser pulse processing: The light path setup of our femtosecond laser pulse processing system was reported in our previous study.[8]

Characterization of MoS_2 nanostructures: The optical images were obtained using an Olympus microscope. The AFM characterization was carried out using a SPM-960 AFM. The SEM images and EDX mapping spectra were obtained using a Hitachi scanning electron microscope. Raman spectra were obtained using a Renishaw InVia Reflex spectrometer (532 nm light source). XPS was performed using a PHI Quantera X-ray photoelectron spectrometer.

Device fabrication and electrical characterization: Multilayer MoS_2 flakes were placed on p+Si/SiO_2 (300 nm) substrates and processed by femtosecond laser pulse. Then the substrates were spin-coated with poly methyl methacrylate (PMMA) solution. The source and drain electrodes were fabricated through three main steps: standard electron-beam lithography (EBL) was performed by Zeiss Supra55 SEM and Raith pattern generator to pattern the PMMA masks; 5 nm Ti/75 nm Au were deposited through electronic beam evaporation; a lift-off process was performed in acetone. The electrical measurements of the fabricated MoS_2 FET were performed by using a Keithley 4200 semiconductor characterization system in air and at room temperature.

ASSOCIATED CONTENT

Supporting Information. The Supporting Information is available free of charge on the ACS Publications website.

Supplementary XPS Mo, O, and S spectra of pristine MoS_2, XPS S spectra of FLP-MoS_2, and supplementary electrical test results of MoS_2 FETs with moderate surface modification by femtosecond laser pulses (PDF).

AUTHOR INFORMATION

Corresponding Author

*E-mail (Xin Li): lixin02@bit.edu.cn.

Author Contributions

The manuscript was written through contributions of all authors. All authors have given approval to the final version of the manuscript.

Funding Sources

National Key R&D Program of China (Grant No. 2017YFB1104300), National Natural Science Foundation of China (Grant No. 51775047), and China Postdoctoral Science Foundation Funded Project (Grant No. BX20190037).

Notes

The authors declare no competing financial interest.

ACKNOWLEDGMENT

The research was supported by the National Key R&D Program of China (Grant No. 2017YFB1104300), National Natural Science Foundation of China (Grant No. 51775047), and China Postdoctoral Science Foundation Funded Project (Grant No. BX20190037).

REFERENCES

1. Chhowalla, M.; Jena, D.; Zhang, H., Two-dimensional semiconductors for transistors. *Nature Reviews Materials* **2016,** *1*, 16052.

2. Bertolazzi, S.; Bonacchi, S.; Nan, G.; Pershin, A.; Beljonne, D.; Samorì, P., Engineering Chemically Active Defects in Monolayer MoS2 Transistors via Ion-Beam Irradiation and Their Healing via Vapor

Deposition of Alkanethiols. *Advanced Materials* **2017,** *29* (18), 1606760.

3. Nam, H.; Wi, S.; Rokni, H.; Chen, M.; Priessnitz, G.; Lu, W.; Liang, X., MoS2 Transistors Fabricated via Plasma-Assisted Nanoprinting of Few-Layer MoS2 Flakes into Large-Area Arrays. *ACS Nano* **2013,** *7* (7), 5870-5881.

4. Eda, G.; Maier, S. A., Two-dimensional crystals: managing light for optoelectronics. *ACS Nano* **2013,** *7* (7), 5660-5665.

5. Mak, K. F.; He, K.; Lee, C.; Lee, G. H.; Hone, J.; Heinz, T. F.; Shan, J., Tightly bound trions in monolayer MoS2. *Nat. Mater.* **2013,** *12* (3), 207-211.

6. Yu, Y.; Ji, Z.; Zu, S.; Du, B.; Kang, Y.; Li, Z.; Zhou, Z.; Shi, K.; Fang, Z., Ultrafast Plasmonic Hot Electron Transfer in Au Nanoantenna/MoS2 Heterostructures. *Adv. Funct. Mater.* **2016,** *26* (35), 6394-6401.

7. Behura, S.; Berry, V., interfacial nondegenerate doping of MoS2 and other two-dimensional semiconductors. *ACS Nano* **2015,** *9* (3), 2227-2230.

8. Zuo, P.; Jiang, L.; Li, X.; Li, B.; Ran, P.; Li, X.; Qu, L.; Lu, Y., Metal (Ag, Pt)–MoS2 Hybrids Greenly Prepared Through Photochemical Reduction of Femtosecond Laser Pulses for SERS and HER. *ACS Sustainable Chemistry & Engineering* **2018,** *6* (6), 7704-7714.

9. Lu, J.; Liu, H.; Tok, E. S.; Sow, C.-H., Interactions between lasers and two-dimensional transition metal dichalcogenides. *Chem. Soc. Rev.* **2016,** *45* (9), 2494-2515.

10. Cho, K.; Pak, J.; Kim, J.-K.; Kang, K.; Kim, T.-Y.; Shin, J.; Choi, B. Y.; Chung, S.; Lee, T., Contact-Engineered Electrical Properties of MoS2 Field-Effect Transistors via Selectively Deposited Thiol-Molecules. *Advanced Materials* **2018,** *30* (18), 1705540.

11. Cheng, R.; Jiang, S.; Chen, Y.; Liu, Y.; Weiss, N.; Cheng, H.-C.; Wu, H.; Huang, Y.; Duan, X., Few-layer molybdenum disulfide transistors and circuits for high-speed flexible electronics. *Nature Communications* **2014,** *5*, 5143.

12. Gao, G.; Wan, B.; Liu, X.; Sun, Q.; Yang, X.; Wang, L.; Pan, C.; Wang, Z. L., Tunable Tribotronic Dual-Gate Logic Devices Based on 2D MoS2 and Black Phosphorus. *Advanced Materials* **2018,** *30* (13), 1705088.

13. Yoo, H.; Hong, S.; On, S.; Ahn, H.; Lee, H.-K.; Hong, Y. K.; Kim, S.; Kim, J.-J., Chemical Doping Effects in Multilayer MoS2 and Its Application in Complementary Inverter. *ACS Applied Materials & Interfaces* **2018,** *10* (27), 23270-23276.

14. Pak, Y.; Park, W.; Mitra, S.; Sasikala Devi, A. A.; Loganathan, K.; Kumaresan, Y.; Kim, Y.; Cho, B.; Jung, G.-Y.; Hussain, M. M.; Roqan, I. S., Enhanced Performance of MoS2 Photodetectors by Inserting an ALD-Processed TiO2 Interlayer. *Small* **2018,** *14* (5), 1703176.

15. Woo, Y.; Hong, W.; Yang, S. Y.; Kim, H. J.; Cha, J.-H.; Lee, J. E.; Lee, K. J.; Kang, T.; Choi, S.-Y., Large-Area CVD-Grown MoS2 Driver Circuit Array for Flexible Organic Light-Emitting Diode Display. *Advanced Electronic Materials* **2018,** *0* (0), 1800251.

16. Choi, M.; Park, Y. J.; Sharma, B. K.; Bae, S.-R.; Kim, S. Y.; Ahn, J.-H., Flexible active-matrix organic light-emitting diode display enabled by MoS₂ thin-film transistor. *Science Advances* **2018,** *4* (4).

17. Zhang, J.; Lang, X. Y.; Zhu, Y. F.; Jiang, Q., Strain tuned InSe/MoS2 bilayer van der Waals heterostructures for photovoltaics or photocatalysis. *Physical Chemistry Chemical Physics* **2018,** *20* (26), 17574-17582.

18. Xu, M.; Chen, Y.; Xiong, F.; Wang, J.; Liu, Y.; Lv, J.; Li, Y.; Wang, Y.; Chen, Z.; Ma, Y., A hidden symmetry-broken phase of MoS2 revealed as a superior photovoltaic material. *Journal of Materials*

Chemistry A **2018,** *6* (33), 16087-16093.

19. Chen, Q.; Lu, J.; Liang, L.; Zheliuk, O.; Ali El Yumin, A.; Ye, J., Continuous Low-Bias Switching of Superconductivity in a MoS2 Transistor. *Advanced Materials* **2018,** *30* (28), 1800399.

20. Saito, Y.; Nakamura, Y.; Bahramy, M. S.; Kohama, Y.; Ye, J.; Kasahara, Y.; Nakagawa, Y.; Onga, M.; Tokunaga, M.; Nojima, T.; Yanase, Y.; Iwasa, Y., Superconductivity protected by spin–valley locking in ion-gated MoS2. *Nature Physics* **2015,** *12*, 144.

21. Kumar, R.; Goel, N.; Kumar, M., UV-Activated MoS2 Based Fast and Reversible NO2 Sensor at Room Temperature. *ACS Sensors* **2017,** *2* (11), 1744-1752.

22. Ryu, B.; Nam, H.; Oh, B.-R.; Song, Y.; Chen, P.; Park, Y.; Wan, W.; Kurabayashi, K.; Liang, X., Cyclewise Operation of Printed MoS2 Transistor Biosensors for Rapid Biomolecule Quantification at Femtomolar Levels. *ACS Sensors* **2017,** *2* (2), 274-281.

23. Zhao, J.; Yu, H.; Chen, W.; Yang, R.; Zhu, J.; Liao, M.; Shi, D.; Zhang, G., Patterned Peeling 2D MoS2 off the Substrate. *ACS Applied Materials & Interfaces* **2016,** *8* (26), 16546-16550.

24. Huang, M.; Li, S.; Zhang, Z.; Xiong, X.; Li, X.; Wu, Y., Multifunctional high-performance van der Waals heterostructures. *Nature Nanotechnology* **2017,** *12*, 1148.

25. Radisavljevic, B.; Radenovic, A.; Brivio, J.; Giacometti, V.; Kis, A., Single-layer MoS2 transistors. *Nature Nanotechnology* **2011,** *6*, 147.

26. Cong, R.; Qiao, S.; Liu, J.; Mi, J.; Yu, W.; Liang, B.; Fu, G.; Pan, C.; Wang, S., Ultrahigh, Ultrafast, and Self-Powered Visible-Near-Infrared Optical Position-Sensitive Detector Based on a CVD-Prepared Vertically Standing Few-Layer MoS2/Si Heterojunction. *Advanced Science* **2018,** *5* (2), 1700502.

27. Liu, H.; Zhu, Y.; Meng, Q.; Lu, X.; Kong, S.; Huang, Z.; Jiang, P.; Bao, X., Role of the carrier gas flow rate in monolayer MoS2 growth by modified chemical vapor deposition. *Nano Research* **2017,** *10* (2), 643-651.

28. Liu, K.-K.; Zhang, W.; Lee, Y.-H.; Lin, Y.-C.; Chang, M.-T.; Su, C.-Y.; Chang, C.-S.; Li, H.; Shi, Y.; Zhang, H.; Lai, C.-S.; Li, L.-J., Growth of Large-Area and Highly Crystalline MoS2 Thin Layers on Insulating Substrates. *Nano Letters* **2012,** *12* (3), 1538-1544.

29. Pak, S.; Lee, J.; Lee, Y.-W.; Jang, A. R.; Ahn, S.; Ma, K. Y.; Cho, Y.; Hong, J.; Lee, S.; Jeong, H. Y.; Im, H.; Shin, H. S.; Morris, S. M.; Cha, S.; Sohn, J. I.; Kim, J. M., Strain-Mediated Interlayer Coupling Effects on the Excitonic Behaviors in an Epitaxially Grown MoS2/WS2 van der Waals Heterobilayer. *Nano Letters* **2017,** *17* (9), 5634-5640.

30. Shi, Y.; Zhou, W.; Lu, A.-Y.; Fang, W.; Lee, Y.-H.; Hsu, A. L.; Kim, S. M.; Kim, K. K.; Yang, H. Y.; Li, L.-J.; Idrobo, J.-C.; Kong, J., van der Waals Epitaxy of MoS2 Layers Using Graphene As Growth Templates. *Nano Letters* **2012,** *12* (6), 2784-2791.

31. Xue, Y.; Zhang, Y.; Liu, Y.; Liu, H.; Song, J.; Sophia, J.; Liu, J.; Xu, Z.; Xu, Q.; Wang, Z.; Zheng, J.; Liu, Y.; Li, S.; Bao, Q., Scalable Production of a Few-Layer MoS2/WS2 Vertical Heterojunction Array and Its Application for Photodetectors. *ACS Nano* **2016,** *10* (1), 573-580.

32. Choudhary, N.; Park, J.; Hwang, J. Y.; Chung, H.-S.; Dumas, K. H.; Khondaker, S. I.; Choi, W.; Jung, Y., Centimeter Scale Patterned Growth of Vertically Stacked Few Layer Only 2D MoS2/WS2 van der Waals Heterostructure. *Scientific Reports* **2016,** *6*, 25456.

33. Chen, X.; Park, Y. J.; Das, T.; Jang, H.; Lee, J.-B.; Ahn, J.-H., Lithography-free plasma-induced patterned growth of MoS2 and its heterojunction with graphene. *Nanoscale* **2016,** *8* (33), 15181-15188.

34. Kim, H.-J.; Kim, H.; Yang, S.; Kwon, J.-Y., Grains in Selectively Grown MoS2 Thin Films. *Small* **2017,** *13* (46), 1702256.

35. Han, G. G. D.; Tu, K.-H.; Niroui, F.; Xu, W.; Zhou, S.; Wang, X.; Bulović, V.; Ross, C. A.; Warner, J. H.; Grossman, J. C., Photoluminescent Arrays of Nanopatterned Monolayer MoS2. *Advanced Functional Materials* **2017,** *27* (45), 1703688.

36. Jung, Y.; Shen, J.; Liu, Y.; Woods, J. M.; Sun, Y.; Cha, J. J., Metal Seed Layer Thickness-Induced Transition From Vertical to Horizontal Growth of MoS2 and WS2. *Nano Letters* **2014,** *14* (12), 6842-6849.

37. Mahjouri-Samani, M.; Lin, M.-W.; Wang, K.; Lupini, A. R.; Lee, J.; Basile, L.; Boulesbaa, A.; Rouleau, C. M.; Puretzky, A. A.; Ivanov, I. N.; Xiao, K.; Yoon, M.; Geohegan, D. B., Patterned arrays of lateral heterojunctions within monolayer two-dimensional semiconductors. *Nature Communications* **2015,** *6*, 7749.

38. Cao, L.; Yang, S.; Gao, W.; Liu, Z.; Gong, Y.; Ma, L.; Shi, G.; Lei, S.; Zhang, Y.; Zhang, S.; Vajtai, R.; Ajayan, P. M., Direct Laser-Patterned Micro-Supercapacitors from Paintable MoS2 Films. *Small* **2013,** *9* (17), 2905-2910.

39. Lu, J.; Lu, J. H.; Liu, H.; Liu, B.; Chan, K. X.; Lin, J.; Chen, W.; Loh, K. P.; Sow, C. H., Improved Photoelectrical Properties of MoS2 Films after Laser Micromachining. *ACS Nano* **2014,** *8* (6), 6334-6343.

40. Jiang, L.; Wang, A.-D.; Li, B.; Cui, T.-H.; Lu, Y.-F., Electrons dynamics control by shaping femtosecond laser pulses in micro/nanofabrication: modeling, method, measurement and application. *Light: Sci. Appl.* **2018,** *7* (2), 17134.

41. Wang, M.; Jiang, L.; Wang, S.; Guo, Q.; Tian, F.; Chu, Z.; Zhang, J.; Li, X.; Lu, Y., Multiscale Visualization of Colloidal Particle Lens Array Mediated Plasma Dynamics for Dielectric Nanoparticle Enhanced Femtosecond Laser-Induced Breakdown Spectroscopy. *Analytical Chemistry* **2019**.

42. Huang, M.; Zhao, F.; Cheng, Y.; Xu, N.; Xu, Z., Origin of Laser-Induced Near-Subwavelength Ripples: Interference between Surface Plasmons and Incident Laser. *ACS Nano* **2009,** *3* (12), 4062-4070.

43. Shuangshuang, H.; Yanyan, H.; Pingxin, X.; Yi, Z.; Shian, Z.; Tianqing, J.; Zhenrong, S.; Jianrong, Q.; Zhizhan, X., Formation of long- and short-periodic nanoripples on stainless steel irradiated by femtosecond laser pulses. *Journal of Physics D: Applied Physics* **2011,** *44* (50), 505401.

44. Xia, B.; Jiang, L.; Li, X.; Yan, X.; Zhao, W.; Lu, Y., High aspect ratio, high-quality microholes in PMMA: a comparison between femtosecond laser drilling in air and in vacuum. *Applied Physics A* **2015,** *119* (1), 61-68.

45. Paradisanos, I.; Kymakis, E.; Fotakis, C.; Kioseoglou, G.; Stratakis, E., Intense femtosecond photoexcitation of bulk and monolayer MoS2. *Applied Physics Letters* **2014,** *105* (4), 041108.

46. Serincan, U.; Kartopu, G.; Guennes, A.; Finstad, T. G.; Turan, R.; Ekinci, Y.; Bayliss, S. C., Characterization of Ge nanocrystals embedded in SiO 2 by Raman spectroscopy. *Semiconductor Science and Technology* **2004,** *19* (2), 247.

47. Nesheva, D.; Raptis, C.; Perakis, A., Raman scattering and photoluminescence from Si nanoparticles in annealed SiOx thin films. *Journal of Applied Physics* **2002,** *92* (8), 4678-4683.

48. Wei, X.; Yu, Z.; Hu, F.; Cheng, Y.; Yu, L.; Wang, X.; Xiao, M.; Wang, J.; Wang, X.; Shi, Y., Mo-O bond doping and related-defect assisted enhancement of photoluminescence in monolayer MoS2. *AIP Adv.* **2014,** *4* (12), 123004.

49. da Silveira Firmiano, E. G.; Rabelo, A. C.; Dalmaschio, C. J.; Pinheiro, A. N.; Pereira, E. C.; Schreiner, W. H.; Leite, E. R., Supercapacitor electrodes obtained by directly bonding 2D MoS2 on reduced graphene oxide. *Adv. Energy Mater.* **2014,** *4* (6).

50. Hollinger, G., Structures chimique et electronique de l'interface SiO2-Si. *Applications Surf. Sci.* **1981,** *8* (3), 318-336.

51. Shuxian, Z.; Hall, W. K.; Ertl, G.; Knözinger, H., X-ray photoemission study of oxygen and nitric oxide adsorption on MoS2. *J. of Catal.* **1986,** *100* (1), 167-175.

52. Finster, J.; Klinkenberg, E.-D.; Heeg, J.; Braun, W., ESCA and SEXAFS investigations of insulating materials for ULSI microelectronics. *Vacuum* **1990,** *41* (7-9), 1586-1589.

53. Colton, R. J.; Guzman, A. M.; Rabalais, J. W., Electrochromism in some thin ‐ film transition ‐ metal oxides characterized by x ‐ ray electron spectroscopy. *J. Appl. Phys.* **1978,** *49* (1), 409-416.

54. Chowdari, B.; Tan, K.; Chia, W.; Gopalakrishnan, R., X-ray photoelectron spectroscopic studies of molybdenum phosphate glassy system. *J. Non-cryst. Solids* **1990,** *119* (1), 95-102.

55. Nan, H.; Wang, Z.; Wang, W.; Liang, Z.; Lu, Y.; Chen, Q.; He, D.; Tan, P.; Miao, F.; Wang, X., Strong photoluminescence enhancement of MoS2 through defect engineering and oxygen bonding. *ACS Nano* **2014,** *8* (6), 5738-5745.

56. Zhou, W.; Zou, X.; Najmaei, S.; Liu, Z.; Shi, Y.; Kong, J.; Lou, J.; Ajayan, P. M.; Yakobson, B. I.; Idrobo, J.-C., Intrinsic structural defects in monolayer molybdenum disulfide. *Nano Lett* **2013,** *13* (6), 2615-2622.

57. Yan, Y.; Xia, B.; Ge, X.; Liu, Z.; Wang, J.-Y.; Wang, X., Ultrathin MoS2 nanoplates with rich active sites as highly efficient catalyst for hydrogen evolution. *ACS Appl. Mater. Interfaces* **2013,** *5* (24), 12794-12798.

58. Wang, X.; Zhang, T.-B.; Yang, W.; Zhu, H.; Chen, L.; Sun, Q.-Q.; Zhang, D. W., Improved integration of ultra-thin high-k dielectrics in few-layer MoS2 FET by remote forming gas plasma pretreatment. *Applied Physics Letters* **2017,** *110* (5), 053110.

For Table of Contents Only